

Applicability of real-time PPP technique in polar regions as an accurate and efficient real-time positioning system

Reha Metin ALKAN[†], Serdar EROL, Bilal MUTLU

Department of Geomatics Engineering, Faculty of Civil Engineering, İstanbul Technical University, İstanbul, Türkiye

Received: 28.04.2023 • Accepted/Published Online: 21.10.2023 • Final Version: 28.11.2023

Abstract: The polar regions, which include the Arctic and Antarctic areas, attract the attention of people every day, and issues that are closely related to the future of humanity make these regions even more important. Accurate and reliable positioning in polar regions is very critical for scientific research projects and also for commercial, touristic, and other human activities. In this study, the usability and the accuracy performance of the real-time precise point positioning (RT-PPP) technique in high-latitude polar regions with harsh environmental and extreme atmospheric conditions were investigated. Within that framework, the GNSS dataset of six IGS multi-GNSS stations located at different latitudes in the north and south polar regions and two different Real-Time Service products (precise satellite orbits and clock corrections and biases) were used. The 3D RT-PPP coordinates of the reference stations were estimated for each 1-s epoch during the 26.5-h measurement period (total of approximately 95,000 epochs). The RT-PPP-derived coordinates were calculated using real-time products generated by IGS Centre National D'études Spatiales (CNES) and Spaceop NAVCAST services with different GNSS constellations including GPS-only, Galileo-only, and a combination of GPS and Galileo. It was shown that the RT-PPP technique provides a decimeter to centimeter level of positioning accuracy using data from only one GNSS receiver after the initialization period. The results also proved that RT-PPP performance strongly depended on the real-time products that were used and the GNSS constellation type. This attainable accuracy from the RT-PPP technique can meet the requirements of many Arctic and Antarctic projects. In general, it can be said that the RT-PPP technique has become an alternative to the conventional relative GNSS techniques in remote areas.

Key words: Antarctica, Arctic, polar region, real-time-precise point positioning, IGS-Real-Time Service, NAVCAST

1. Introduction

Scientific studies in the Arctic and Antarctic regions will significantly influence the future of Earth, and they also carry serious importance for the future of humanity. Therefore, interest in these regions is increasing day by day. Many scientists from many different countries, including Türkiye, need robust and reliable highly accurate positioning in their scientific research efforts in the polar regions, including geodetic, geological, geophysical, climate, seismic, oceanographic, glacier, marine, atmospheric, and social sciences research. Using conventional terrestrial surveying techniques in extremely challenging polar environments is generally difficult. Intense ice and snow, extreme cold, strong winds, and bright sun rays affect surveying activities negatively and create many issues related to the safety of the surveyor and the equipment. As an alternative, satellite-based Global Navigation Satellite System (GNSS) positioning techniques have begun to be used for different applications. With the GNSS technique, it is possible to perform positioning with many methods

and approaches, resulting in different levels of accuracy. Among them, real-time single-point positioning (SPP) based on code measurements with a single GNSS receiver provides accuracy in the range of meters. This accuracy may be good enough for purposes such as personal navigation or location-based services, but not for most geodetic applications. In contrast, centimeter-level positioning accuracy requires carrier-phase measurements via application of a differential GNSS algorithm, including postprocessing or real-time modes. To implement this technique, it is necessary to conduct simultaneous observations at reference station(s) or use a reference network whose position is known with high accuracy. For real-time applications, a technique called real-time kinematic (RTK) positioning has been used since the early 1990s. Although the RTK technique is a standard GNSS positioning method for real-time applications, the requirement of simultaneous observations and a robust communication infrastructure for transmitting raw data or real-time corrections to the rover receiver makes the RTK method difficult to use

* Correspondence: alkanr@itu.edu.tr

in challenging polar environments. On the other hand, if postprocessing is required, GNSS data processing software and an expert who can use the software are needed. All these factors affect the productivity of the differential relative GNSS positioning method in both postprocess and real-time modes and increase the time and cost of field studies while decreasing the flexibility of field operations. At the same time, the extreme weather and geographical conditions of the polar regions bring additional challenges in applying this method compared to any other regions.

As a result of the advancements in satellite geodesy and data processing techniques, precise point positioning (PPP) was developed to perform positioning with the accuracy and productivity of the differential GNSS method without the need for a reference station or GNSS network observations. PPP-derived coordinates are estimated by combining data from a single-frequency or multifrequency GNSS receiver along with precise products (satellite clocks and orbit corrections), as well as biases and some other products provided by many data analysis centers around the world, primarily via the International GNSS Service (IGS). Convergence time of dozens of minutes is required to achieve centimeter-level accuracy with the PPP technique (Qu et al., 2023). Achievable accuracy and convergence time may vary based on the data processing strategy (e.g., float or ambiguity-fixed PPP-AR solutions), the type of receiver and antenna, the quality and type of collected data, the GNSS constellation health and availability, the atmospheric activity, the precise products used, and the surveying conditions. The long convergence time requirement of PPP is a serious drawback that severely restricts the use of this technique in real-time applications (An et al., 2023). Finally, real-time precise point positioning (RT-PPP), which combines the PPP and RTK techniques, began with the production of real-time precise products within the scope of the International GNSS Service Real-Time Service (IGS-RTS) project implemented by the IGS in 2013. Since then, employing the PPP technique in real-time applications has been possible with the utilization of real-time products. These real-time products are calculated and formatted according to Radio Technical Commission for Maritime-State Space Representation (RTCM-SSR) standards and distributed in real-time over the internet with the Networked Transport of RTCM via Internet Protocol (NTRIP).

In these challenging Arctic and Antarctic regions, limited academic studies have been conducted on the usability of the PPP technique in both postmission and real-time modes. In one of those studies, Erol et al. (2023) investigated the performance of the RT-PPP technique using a GNSS dataset collected at one of the IGS reference stations located in Antarctica. They tried to calculate 3D RT-PPP coordinates using different real-time products, i.e., IGS

and NAVCAST, and different satellite configurations. Results from that study showed that the combination of GPS and Galileo produced better accuracy than using a single GPS. Savchyn et al. (2023) determined the horizontal deformation of the Antarctic plate by processing data from 60 GNSS stations with the PPP technique. They used the GIPSY-OASIS-II software static PPP module to calculate the coordinates and time series of the handled reference stations. According to their results, the horizontal displacement vector components were determined with accuracies ranging from 0.1 to 3.4 mm. Jin et al. (2023) analyzed the positioning, timing, and short message service performance of the BeiDou-3 Navigation Satellite System (BDS-3) via a newly proposed synthetic method. They collected the GNSS data of a ship moving in the Arctic region. The results obtained from the ship measurements showed that the positioning accuracy of the kinematic PPP method in the polar region was comparable to that of other regions. In another study by Alkan et al. (2022), RT-PPP coordinates were determined with BNC (BKG Ntrip Client) software using only OHI3 GNSS reference station data from the Antarctic region and multi-GNSS IGS real-time precise products. The results of that study, based on a single GNSS station, revealed that after about 30 min of convergence time, the 3D position could be determined with the RT-PPP technique with accuracies ranging from centimeters to decimeters. Cheng et al. (2022) explored PPP performance under different satellite constellations and frequencies using data from 17 different IGS reference stations, including polar regions. According to their results, the static PPP provided centimeter-level accuracy while kinematic solutions provided decimeter-level accuracy. Di et al. (2022) analyzed the performance of RT-PPP based on multi-GNSS observations in the Arctic Northeast Passage. They obtained centimeter- to meter-level positioning accuracy depending on the single- or dual-frequency observations used. Zhao et al. (2022) assessed multi-GNSS positioning performance and signal quality in polar regions by using multi-GNSS observations, including 10 reference stations from the Multi-GNSS Experiment (MGEX) and two reference stations from the International GNSS Monitoring & Assessment System (iGMAS). The collected data were processed with newly developed processing software based on GAMP (GNSS Analysis Software for Multi-constellation and Multi-frequency Precise Positioning). The PPP accuracy was found to be at the centimeter level for the BDS-3-only single constellation. Their results showed that the multiconstellation solution slightly improved the positioning accuracy, reduced the convergence time, and greatly increased the number of visible satellites compared to the system with a single constellation. Fan et al. (2021) focused on the positioning performance of BDS-3 complete system observations in the Arctic and Antarctic re-

gions based on GNSS data from 9 iGMAS stations. They found that the accuracy of BDS-3 B1C UERE was approximately 0.50 m in polar regions. Bezioglu et al. (2019) tested the kinematic performances of postprocessed PPP-AR and PPP-float approaches in an Antarctic marine environment. Based on the results obtained from the CSRS-PPP online GNSS processing service, they concluded that both approaches provided centimeter or decimeter levels of accurate positioning. Li et al. (2019a) implemented a precise orbit positioning (POP) approach for kinematic positioning over Antarctica. They validated POP in comparison to PPP with respect to integer ambiguity-fixing performance and accuracy. Their simulation test was based on observations from 136 globally distributed MGEX reference stations over a 14-day period. The data were then processed epoch by epoch in kinematic mode as if the stations were in motion. They concluded that the POP approach improved ambiguity fixing. According to realistic flight test results, they found that POP also performed better in fixing ambiguity. Li et al. (2019b) applied the POP approach, an extended PPP technique, in a kinematic application for airborne gravity over Antarctica. Data were collected by aircraft and 3D positions were calculated with relative positioning and the PPP technique in addition to the real-time POP approach. According to their results, the derived coordinates generally agreed on the decimeter level. Furthermore, according to the assessment of data from four IGS stations, they found that the PPP solutions had large positioning biases while POP produced more robust solutions. De Jong et al. (2014) tested the performance of PPP in Alaska. Although data were collected at the reference station as static, they were processed in kinematic mode with the PPP algorithm. During this process, GPS data and real-time products generated by Fugro's G2 service were used and PPP-derived coordinates were calculated. They revealed that 2D positions were achieved in the order of a few centimeters in accuracy. For the vertical component, the results were found to be slightly worse than they were for lower latitudes. In another study carried out by Xu et al. (2012), collected airborne kinematic data were processed in PPP mode. Furthermore, the static reference stations' data were also processed in the kinematic mode. Upon analyzing the results, it was found that the mean square error was less than 10 cm. The kinematic processing results of the static reference station data showed that the mean square error was less than 8 cm.

The promising positioning results obtained with this method have enabled many real-time products in state-space representation (SSR) format to be made available for RT-PPP applications by other analysis centers and institutions. Following these improvements, not only IGS but also other services such as NAVCAST and MADOCA (Multi-GNSS Advanced Demonstration Tool for Orbit and Clock

Analysis) have introduced real-time positioning services. A very limited number of academic studies have been conducted to date to investigate the performance of the NAVCAST real-time service. In one of them, Elmezayen and El-Rabbany (2020) found that achieving a subdecimeter level of accuracy in an open-sky environment using NAVCAST precise products was possible. Elmezayen and El-Rabbany (2019) analyzed RT-PPP performance in static and kinematic modes. As a result of the static tests, they found that the contribution of Galileo to the GPS constellation improved the positioning accuracy compared to the GPS-only accuracy and provided centimeter- and decimeter-level accuracy for horizontal positioning and height components, respectively.

In addition to the Spaceopal NAVCAST service, the Japan Aerospace Exploration Agency (JAXA) launched a real-time satellite orbit and clock correction service called MADOCA, which supports GPS, GLONASS, and QZSS systems, in 2014. Yu et al. (2023) assessed the performance of the real-time and offline RT-PPP and PPP-AR techniques using MADOCA products. Centimeter-level positioning accuracy was achieved for static and kinematic PPP using multi-GNSS data and precise products. They concluded that the solution obtained with the PPP-AR technique was superior to the PPP-float solution. In general, the results revealed that positioning accuracy at the decimeter or even centimeter level could be provided by MADOCA products and so this service could meet the demands of RT-PPP solutions. Bezioglu et al. (2021) investigated the performance of the RT-PPP technique using real-time MADOCA products to determine high-rate dynamic motions, seismic waveform, and coseismic displacement. They concluded that RT-PPP was capable of determining dynamic displacement efficiently and safely. Furthermore, it was possible to determine displacement waveforms and the coseismic surface displacement caused by an earthquake with the RT-PPP technique based on MADOCA real-time products.

It should be noted that a continuous and fast internet connection is required to use real-time services properly. The lack of a stable internet connection causes interruptions, which results in more time spent for the reconvergence process. This is a serious limitation in the application of the RT-PPP method. In order to minimize this problem, the RT-PPP technique has begun to be used via satellite-based correction services. In this context, precise satellite orbits and clock offsets, atmospheric corrections (ionospheric and tropospheric), code and carrier phase biases, and other auxiliary information, calculated in real-time using the observations of GNSS tracking stations spread around the world, are transmitted to the mobile rover receiver via satellites using L-band signals or the internet (IP or cellular) in order to perform real-time posi-

tioning with the PPP technique. Delivering precise products via satellite option eliminates the need for cellular coverage, which is especially mandatory for network RTK in challenging environments. CenterPoint RTX (Trimble), Starfix (Fugro), TerraStar (Hexagon/Novatel), Atlas (Hemisphere), and PointPerfect (u-blox) are examples of such services. In general, all of these services provide different levels of accuracy depending on user subscription options between centimeter and meter levels. Today, it is possible to determine centimeter-level ambiguity-fixed solutions almost anywhere in the world without the need for any reference station data or internet connection (Anantakarn and Witchayangkoon, 2019; Lipatnikov and Shevchuk, 2019; Alkan, 2021). As can be seen from the literature, this technology provides productivity and accuracy of RTK positioning while offering seamless and reliable 3D real-time positioning in various applications around the world using only a single GNSS receiver. However, most of these services broadcast the corrections via geostationary satellites, and these satellites cannot be observed in high-latitude regions. Accordingly, the availability of the correction signals is limited. In these cases, the positioning performance decreases compared to studies performed at lower latitudes (Alkan et al., 2022). This limits the use of these services in high-latitude regions. In addition, a paid subscription is required to use these services.

Although many scholars have studied the potential usability of the RT-PPP technique in many application areas in both static and kinematic modes (Wang et al., 2018; Grinter et al., 2020; Liu et al., 2020; Teunissen, 2021; Li X et al., 2022a; Li X et al., 2022b; An et al., 2023; Atiz et al., 2023), very limited research has been conducted in the Antarctic and Arctic polar regions. In this study, unlike the studies in the literature presented above, RT-PPP performance was evaluated in terms of accuracy and conver-

gence time using data from IGS reference stations selected in the Arctic and Antarctic regions, together with precise corrections obtained from different real-time services. The effects of different ambiguity solution algorithms on the results were also investigated by comparing solutions obtained with the PPP-AR and PPP-float approaches. This study is expected to make a significant contribution to the literature's limited information on the usability of the RT-PPP method in polar regions.

2. IGS and NAVCAST real-time precise point positioning (RT-PPP) services

Various public and private initiatives have started offering real-time PPP services. The most prominent among them is IGS-RTS. Thanks to IGS-RTS precise products (i.e., precise satellite orbits and clock offsets, biases, VTEC, and some other auxiliary information) provided by this service, which was officially launched in 2013, subscribed users can perform real-time PPP on a global basis. Until recently, many IGS analysis centers (e.g., BKG, CAS, CNES, DLR/GSOC, ESA/ESOC, GFZ, GMV, NRCan, SHAO, UPC, and WUHAN) operating under the umbrella of IGS-RTS were producing only GPS real-time precise products. Currently, however, precise products for all GNSS constellations, including GLONASS, Galileo, and BDS, are produced and offered free of charge to subscribed users. The IGS-RTS service produces precise products by tracking a global network of more than 300 reference stations. IGS-RTS, as a real-time PPP service, transmits SSR corrections only through the internet, not via satellites. The contributing solutions of IGS analysis centers are given in Table 1. It should be noted that the precise orbits and clock products are streamed with 5-s update intervals. Please also note that G, R, E, and C represent GPS, GLONASS, Galileo, and BDS, respectively.

Table 1. IGS-RTS analysis centers and corresponding precise products (Url-1).

Analysis center	RT orbits and clocks	Other information
BKG	G, R, E	-
CAS	G, R, E, C	VTEC based on GIM
CNES	G, R, E, C	VTEC based on GIM
DLR/GSOC	G, R, E, C, J	-
ESA/ESOC	G	-
GFZ	G, R, E, C	-
GMV	G, R, E, C	-
NRCan	G	-
SHAO	G	-
UPC	-	VTEC based on GIM
WUHAN	G, R, E, C	VTEC based on GIM

One of these IGS analysis centers, CNES, has been producing phase biases as part of the PPP-WIZARD Project since 2014. These biases are compatible with the PPP ambiguity resolution approach. Thus, the PPP-WIZARD software described in the following section provides PPP-ambiguity resolution (PPP-AR) solutions while using CNES phase bias products. PPP-AR solutions reduce the convergence time and improve the overall accuracy of RT-PPP solutions compared to conventional PPP-float solutions.

Besides IGS-RTS, there are other services that produce freely available real-time precise products for RT-PPP positioning services. Spaceopal GmbH in Germany announced a real-time high-accuracy positioning service called NAVCAST in October 2018. Real-time products are generated using observations from Galileo and GPS constellations at more than 100 globally distributed reference stations. The service produces real-time products, i.e., orbit and clock corrections and both code and phase biases, to remove the GPS and Galileo constellation system errors in the context of the PPP technique. These products are generated using the REal-TIme CLock Estimation (RETICLE) algorithm developed by the German Space Operations Center of DLR. The coded corrections in RTCM 3 format are broadcast over the internet using NTRIP 2.0. As of today, NAVCAST supports Galileo E1, E5a, and E5b, as well as GPS L1, L2, and L5 signals. The orbit corrections update rate is 30 s, while the clock corrections update rate is 5 s. Users require both an NTRIP client and a PPP engine in order to obtain 3D positioning in the centimeter-level range for static and kinematic applications. The NTRIP client receives streams by connecting to the NTRIP caster, while the PPP engine is a software that retrieves the NAVCAST real-time products to calculate the PPP coordinates. The convergence time varies from minutes to half an hour depending on the measurement conditions. Up-to-date and detailed information about the service can be found at the Spaceopal website (Url-2)¹.

In this study, since RT-PPP solutions were obtained with PPP-WIZARD (With Integer and Zero-difference Ambiguity Resolution Demonstrator) software (Laurichesse and Privat 2015), some information about the software and its mathematical algorithm is given below. This open-source software developed by the CNES (Centre National D'études Spatiales) is not only PPP-client software but also a product generator. The PPP-WIZARD software estimates RT-PPP coordinates based on an undifferenced and uncombined functional model. The uncombined phase bias values ($\bar{b}_{\phi_1}^s, \bar{b}_{\phi_2}^s, \bar{b}_{\phi_5}^s$) to be used for the real-time PPP-AR solution on the user side are formed in the network side by using code biases ($\bar{b}_{P_1}^s, \bar{b}_{P_2}^s, \bar{b}_{P_5}^s$), integer phase clocks (dt_{IRC}^s), and wide-lane (WL) satellite biases (μ_{12}^s, μ_{25}^s) in what is also known as the integer re-

covery clock (IRC) model. To perform the transform from the IRC to uncombined phase bias values, the Melbourne-Wübbena (MW) and dual-frequency iono-free (IF) functions are used. The integer property of ambiguity can be fixed by applying the uncombined code and phase biases to the related observation equations below with corrected dt_{IGS}^s (IGS satellite clock error). In Eq. (1), phase (ϕ) and code (P) observation formulas between any satellite s and receiver r for frequencies ($i=1, 2$, and 5) are given.

$$\begin{aligned} P_1 + \bar{b}_{P_1}^s &= \rho_{r,1}^s + c\bar{d}t_r + m^s zwd_r + \gamma_1 \bar{I}_1^s + \varepsilon_{P_1}^s \\ P_2 + \bar{b}_{P_2}^s &= \rho_{r,2}^s + c\bar{d}t_r + m^s zwd_r + \gamma_2 \bar{I}_1^s + \varepsilon_{P_2}^s \\ P_5 + \bar{b}_{P_5}^s &= \rho_{r,5}^s + c\bar{d}t_r + m^s zwd_r + \gamma_5 \bar{I}_1^s + IFB_r + \varepsilon_{P_5}^s \\ \lambda_1 (\phi_1 + \bar{b}_{\phi_1}^s) &= \rho_{r,1}^s + c\bar{d}t_r + m^s zwd_r - \gamma_1 \bar{I}_1^s + \lambda_1 \bar{N}_1^s + \varepsilon_{\phi_1}^s \\ \lambda_2 (\phi_2 + \bar{b}_{\phi_2}^s) &= \rho_{r,2}^s + c\bar{d}t_r + m^s zwd_r - \gamma_2 \bar{I}_1^s + \lambda_2 (\bar{N}_W^s + \bar{N}_1^s) + \varepsilon_{\phi_2}^s \\ \lambda_5 (\phi_5 + \bar{b}_{\phi_5}^s) &= \rho_{r,5}^s + c\bar{d}t_r + m^s zwd_r - \gamma_5 \bar{I}_1^s + \lambda_5 (\bar{N}_E^s + \bar{N}_W^s + \bar{N}_1^s) + \varepsilon_{\phi_5}^s \end{aligned} \quad (1)$$

$$\begin{cases} \alpha_{12} = f_1^2 / (f_1^2 - f_2^2); \beta_{12} = -f_2^2 / (f_1^2 - f_2^2) \\ b_{P_{IF}}^s = \alpha_{12} b_{P_1}^s + \beta_{12} b_{P_2}^s; b_{r,P_{IF}} = \alpha_{12} b_{r,P_1} + \beta_{12} b_{r,P_2} \\ DCB_{r,12} = b_{r,P_1} - b_{r,P_2} \\ \bar{I}_1^s = I_1^s + \beta_{12} DCB_{r,12} \\ c\bar{d}t_r = c dt_r + b_{r,P_{IF}} \\ IFB_r = b_{r,P_5} - b_{r,P_{IF}} - \gamma_5 \beta_{12} DCB_{r,12} \\ \lambda_1 \bar{N}_1^s = \lambda_1 (N_1^s + b_{r,\phi_1}) - b_{r,P_{IF}} + \beta_{12} DCB_{r,12} \\ \lambda_2 (\bar{N}_W^s + \bar{N}_1^s) = \lambda_2 (N_2^s + b_{r,\phi_2}) - b_{r,P_{IF}} + \gamma_2 \beta_{12} DCB_{r,12} \\ \lambda_5 (\bar{N}_E^s + \bar{N}_W^s + \bar{N}_1^s) = \lambda_5 (N_5^s + b_{r,\phi_5}) - b_{r,P_{IF}} + \gamma_5 \beta_{12} DCB_{r,12} \end{cases} \quad (2)$$

In Eqs. (1) and (2), $\rho_{r,i}^s$ is the geometrical distance (including wind-up and relativistic effects) at frequency i (m), c is the speed of light (m/s), dt_r is the receiver clock error (s), $\gamma_i = (f_1/f_i)^2$ is a frequency-dependent scale, I_1^s is the slant ionospheric delay at frequency f_1 (m), m^s is a wet mapping function, zwd_r is wet zenith tropospheric delay (m), b_{r,P_i} and $b_{P_i}^s$ are respectively the receiver and satellite code hardware delays (m), b_{r,ϕ_i} and $b_{\phi_i}^s$ are respectively the receiver and satellite carrier phase hardware delays (m), and ε represents nonmodeled errors (m). $DCB_{r,12}$ is the difference code bias value between P_1 and P_2 signals for receiver r (m). \bar{N}_E^s, \bar{N}_W^s , and \bar{N}_1^s are integer ambiguities for extra-wide-lane, wide-lane, and N_1 , respectively. Please see Liu et al. (2020) and Gazzino et al. (2023) for more information about the mathematical model of the PPP-WIZARD software.

According to the given model, users can obtain RT-PPP-AR solutions using PPP-WIZARD software by applying the code, phase bias products, satellite orbit, and clock corrections, which are broadcast by CNES, directly to raw measurements.

3. Materials and methods

3.1. Description of the study area and data collection

In this study, the performance of the RT-PPP technique in terms of accuracy and convergence time was assessed un-

¹ Url-2. Spaceopal, a DLR Gesellschaft für Raumfahrtanwendungen (GfR) and Telespazio Company, <https://spaceopal.com> [last accessed September 2, 2023].

der the extreme conditions of the Arctic and Antarctic polar regions. Within this framework, real-time data of NABG (78.943°N, 11.857°E), UTQI (71.323°N, 156.615°W), and REYK (64.139°N, 21.955°W) from IGS-RTS network reference stations located in and around the Arctic Circle and OHI3 (63.321°S, 57.901°W), DAV1 (68.577°S, 77.973°E), and SCTB (77.849°S, 166.758°E) from IGS-RTS network reference stations located in and around the Antarctic Circle were selected for the experiments (Figure 1). Some information about the selected stations is given in Table 2. Other detailed information can be found on the IGS website at <https://network.igs.org/#station-map-list>.

3.2. Data processing

The RT-PPP coordinates of the reference stations were calculated epoch by epoch at 1-s intervals using the GNSS observations, broadcast ephemerides, and SSR correction products streamed by the IGS-RTS CNES and Spaceopal NAVCAST-RTS services using different GNSS constellations including GPS-only, Galileo-only, and the combination of GPS and Galileo lasting over 1 day of a measurement

period (~26.5 h) between 24 and 25 October 2022 (GPS days of the year: 297 and 298). It should be noted that the IGS and NAVCAST streams were freely available after registration.

It is also worth mentioning that since the NAVCAST service produces corrections for only GPS and Galileo constellations, we only used the GPS and Galileo observations in the RT-PPP solutions, although the reference stations track the constellations of other satellites as well. The PPP-AR algorithm was applied for RT-PPP solutions using CNES products and the PPP-float approach was applied for RT-PPP solutions using NAVCAST products. The PPP-WIZARD software was used as a PPP engine to retrieve the NAVCAST and IGS products through NTRIP to calculate real-time PPP coordinates. The parameters and correction models used in the solutions are given in Table 3. Detailed information on the models and corrections applied by PPP-WIZARD has been given by Laurichesse and Privat (2015), Ding et al. (2017), Liu et al. (2020), and Gazzino et al. (2023).

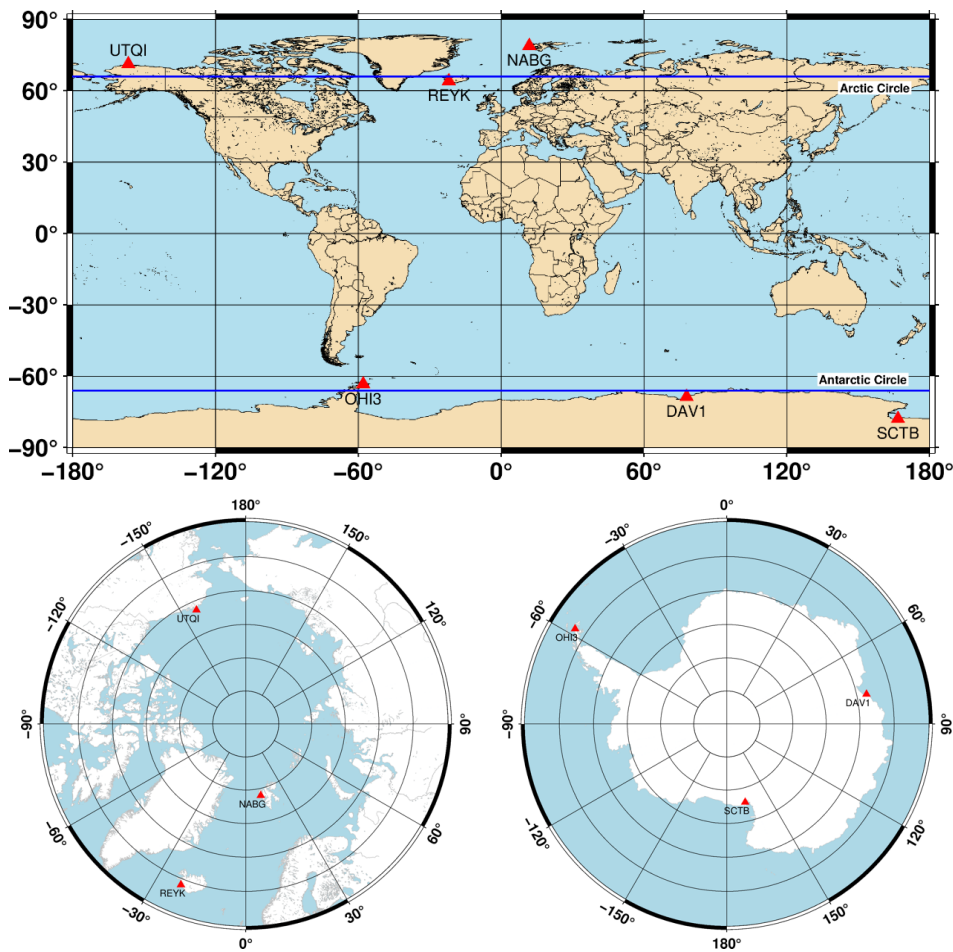
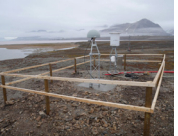



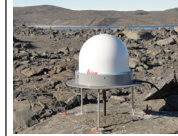



Figure 1. Distribution of the used IGS-MGEX RTS reference stations in polar regions.

Table 2. Used reference stations' information (from <https://igs.org/network/#station-map-list>).

Site	NABG	UTQI	REYK	OHI3	DAV1	SCTB
Site name	Ny-Alesund Brandallaguna G	Utqiagvik	Reykjavik	O'Higgins	Davis	Scott Base
City or town / country	Ny-Alesund / Norway	Utqiagvik / Alas- ka, USA	Reykjavik / Ice- land	O'Higgins / Antarctica	Davis / Antarctica	Scott Base / Ant- arctica
Monument description	Steel mast	Steel platform	Concrete	Pillar	Stainless steel plate	Mast
Approximate coordinates	78.943°N 11.857°E 43 m	71.323°N 156.615°W 12 m	64.139°N 21.955°W 93 m	63.321°S 57.901°W 32 m	68.577°S 77.973°E 45 m	77.849°S 166.758°E -19 m
Receiver and antenna type	TRIMBLE NETR9 TRM59900.00	JAVAD TR_G3TH JAV_GRANT- G3T	LEICA GR50 LEIAR25.R4	LEICA GR50 LEIAR25.R4	SEPT POLARX5 LEIAR25.R3	TRIMBLE AL- LOY TRM115000.00
Satellite systems*	G+R+E+C	G+R+E	G+R+E+C+I+S	G+R+E+C+S	G+R+E+C+I+J	G+R+E+C+J
Location	In Arctic Circle	In Arctic Circle	Near Arctic Circle	Near Antarctic Circle	In Antarctic Circle	In Antarctic Circle
Photo						

* G: GPS, R: GLONASS, E: Galileo, C: BDS, I: IRNSS, J: QZSS, S: SBAS.

3.3. Numerical results

The signal quality indicators of the data collected during the test measurements and other processing results are given in the following subsections.

3.3.1. Number of satellites and PDOP assessment as signal quality indicator

Observed numbers of satellites (NofSAT) are given in Table 4. Considering the values given in Table 4, at least 4 and a maximum of 14 satellites were observed for GPS (10 as the mean), while for Galileo, at least 5 and a maximum of 11 (8 as the mean) satellites were observed. With the combination of both systems, the total number of satellites was obtained as at least 11 and at most 23 (an average of 18). As can be seen, the GPS + Galileo combination significantly increased the number of satellites. This is very important in terms of signal availability, reliability, and coverage in harsh polar environments. Additionally, more satellites improved the spatial geometry of GNSS satellites and thus improved the positioning accuracy.

The spatial geometry of the tracked satellites and user receiver can be expressed by dilution of precision (DOP) values, and they are thus an important source of information about the user's 3D positioning accuracy. Within this framework, the position dilution of precision (PDOP) values were calculated and are given in Table 5.

The numerical results showed that, in general, the GPS-only observations had better PDOP values than the Galileo-only observations. As can be seen in Table 5, it was observed that when Galileo satellites were used together with GPS satellites, PDOP values were improved by an average of 33% compared to GPS-only values and an average of 39% compared to Galileo-only values. Overall, it was concluded that using Galileo in combination with GPS made a significant contribution compared to a single satellite system.

Additionally, GPS, Galileo, and GPS + Galileo sky plots of GNSS satellites observed for all reference stations, from the northernmost to the southernmost during the measurement period, are presented in Figure 2.

As can be seen clearly from Figure 2, no GPS or Galileo satellites were observed in the zenith direction of all stations in both the Arctic and Antarctic regions. Since the orbital planes of the satellites are inclined at 55° for GPS and 56° for Galileo relative to the equator, observations cannot be made in the zenith directions of the stations with latitude values above these inclination angles. As a result, an unobservable area (a circular hole) occurs in the sky above the reference stations. This will reduce the positioning accuracy, especially for the height component (Jensen and Sicard, 2010).

Table 3. Processing strategy applied in this study.

Items	Descriptions (for CNES / NAVCAST solutions)
RT-Service	IGS-CNES / Spaceopal NAVCAST
PPP-Client software	PPP-WIZARD v.1.4.3
GNSS satellites	G, E, G+E
GNSS observations	Undifferenced, uncombined raw code and phase
Solution strategy	RT-PPP
Ambiguity	Fixed (PPP-AR) / Float (PPP-float)
Sampling interval	1-s (1 Hz)
Satellite elevation cut-off	7°
Weighting	Elevation-dependent weighting strategy ($1/\sin^2(\text{elevation angle})$): standard deviation of the phase and code observations are 0.01 m and 1 m for both GPS and Galileo in the zenith direction
Mapping function	$1/\sin(\text{elevation angle})$
Antenna phase center corrections	igs14.atx
Streamed precise products	SSRA00CNE0 / CLKA0_DEU1
Streamed broadcast ephemerides	BCEP00BKG0 / BCEP0_DEU1
Priori tropospheric model	Saastamoinen
Phase wind-up	Applied
Solid earth tide	Applied
Relativistic effects	Applied
Parameters estimator	Kalman filter
Tropospheric delay	Estimated
Ionospheric delay	Estimated
Reference frame	ITRF2014

Table 4. Numbers of observed satellites (NofSat).

NofSAT	NABG			UTQI			REYK		
	Min.	Max.	Mean	Min.	Max.	Mean	Min.	Max.	Mean
G	9	13	10	7	13	11	6	12	10
E	6	10	8	6	11	9	5	9	8
G+E	16	22	18	15	23	19	13	21	18
	OHI3			DAV1			SCTB		
G	4	14	10	7	13	10	8	13	10
E	6	9	8	6	11	9	6	10	8
G+E	11	22	18	16	23	19	16	21	18

Considering the elevation angles of the satellites, it was seen that the maximum observed satellite elevation angle decreased as the latitude values of the stations increased. For example, the highest GPS satellite values were observed with a maximum angle of 60° at the NABG station, 70° at the UTQI station, and 85° at the REYK station in

the Arctic region. A similar situation was observed for the OHI3, DAV1, and SCTB stations selected in the Antarctic region. Furthermore, it was seen that the Galileo satellites were observed at slightly higher elevation angles than the GPS satellites. The most likely reason for this is that, as explained above, the orbital inclination of the Galileo sat-

Table 5. PDOP values of observations.

PDOP	NABG			UTQI			REYK		
	Min.	Max.	Mean	Min.	Max.	Mean	Min.	Max.	Mean
G	1.5	4.1	2.2	1.4	4.5	2.1	1.4	6.3	1.9
E	1.7	8.3	2.6	1.5	5.7	2.2	1.5	5.6	2.2
G+E	1.2	2.1	1.5	1.1	2.0	1.4	1.0	2.1	1.3
	OHI3			DAV1			SCTB		
G	1.4	51.4	2.0	1.3	4.3	2.0	1.5	4.2	2.2
E	1.6	4.3	2.2	1.5	3.6	2.1	1.7	7.8	2.4
G+E	1.1	2.1	1.3	1.0	2.0	1.3	1.2	2.2	1.5

ellites, which is 56°, had a slightly larger (1°) inclination angle than that of the GPS satellites, which was 55°.

3.3.2. Status of geomagnetic and solar activity

The ionosphere in the polar regions, which are also referred to as the polar ionosphere or high-latitude ionospheric regions, is extremely unstable (Junior, 2017). The ionospheric scintillations caused by geomagnetic and solar activities affect GNSS performance, especially in polar regions, while reducing GNSS signal quality. As a result of this effect, frequent loss of signal lock occurs in GNSS tracking, which causes cycle slips and phase transitions (Li W et al., 2022). With respect to this, geomagnetic activity index (Kp), disturbance storm time (Dst) index, and solar radio flux (F10.7) index values were calculated and are shared in Figure 3 to allow an examination of ionospheric irregularities in the relevant measurements.

When the geomagnetic activity index (Kp) values given in Figure 3 were examined, it was seen that the average value was approximately 1. According to Poole (2002), Kp values between 0 and 1 indicate quiet magnetic conditions. It should be noted here that if the Kp value is 5 or above, it is only possible to discuss a geomagnetic storm. From this point of view, there was no significant geomagnetic activity throughout the test measurements. It can be seen in Figure 3 that the Dst values, which characterize the level of geomagnetic activity, varied between -10 and +8 nT over the test period. According to these values, geomagnetic activity had no negative effect on the measurements because only Dst values lower than -50 nT indicate high geomagnetic activity. The solar radio flux (F10.7) index is an excellent indicator of the presence of solar activity. It can be seen in Figure 3 that the solar flux index value was about 115 solar flux units (sfu) during the test measurements. This indicates a low level of solar activity.

All of these analyses showed that there were neither geomagnetic nor solar activities at a significant level that would have a negative impact on GNSS data.

3.3.3. Accuracy assessment of RT-PPP-derived coordinates

For the accuracy assessment of the obtained RT-PPP solutions using IGS CNES and NAVCAST SSR products for three different constellation alternatives, the estimated coordinates were compared to the known coordinates of the reference stations. Since the coordinates of all stations were not available for the ITRF14 solution, the known coordinates were calculated with the Canadian Spatial Reference System Precise Point Positioning (CSRS-PPP) online GNSS processing service. That service, operated by Natural Resources Canada, calculates the PPP coordinates using single and/or dual frequency GPS and GLONASS (if available) data collected in static/kinematic modes. The long observation sessions (24+ h) in static mode provide millimeter-level accuracy with CSRS-PPP (Banville, 2020; Url-3). The processing results showed that the coordinates were estimated with millimeter-level precision by fixing most of the GPS integer ambiguities. The differences between calculated and known coordinates for solutions via GPS, Galileo, and the combination of GPS and Galileo are plotted as time series in Figure 4 for the north, east, 2D position, and height components.

In order to assess the accuracy performance of RT-PPP solutions, the root mean square error (RMSE) values of the 2D position and height components were calculated and are given in Table 6.

One of the performance indicators of the PPP technique is convergence time. In this study, the time interval between the first measurement epoch, in which the 2D coordinate positioning differences were below 10 cm, and the

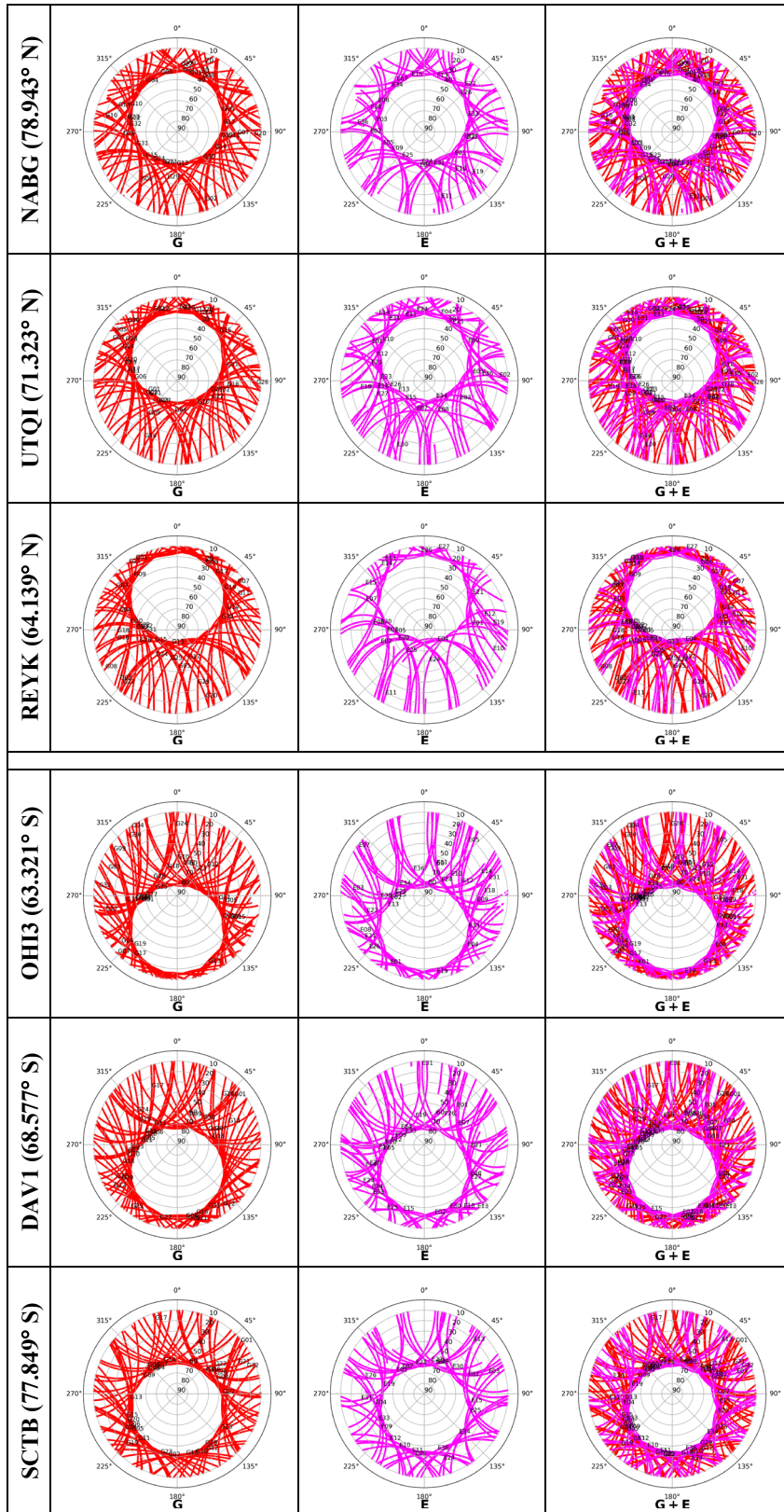


Figure 2. Sky plots of GPS and Galileo satellites tracked over the reference stations at 10° elevation angle.

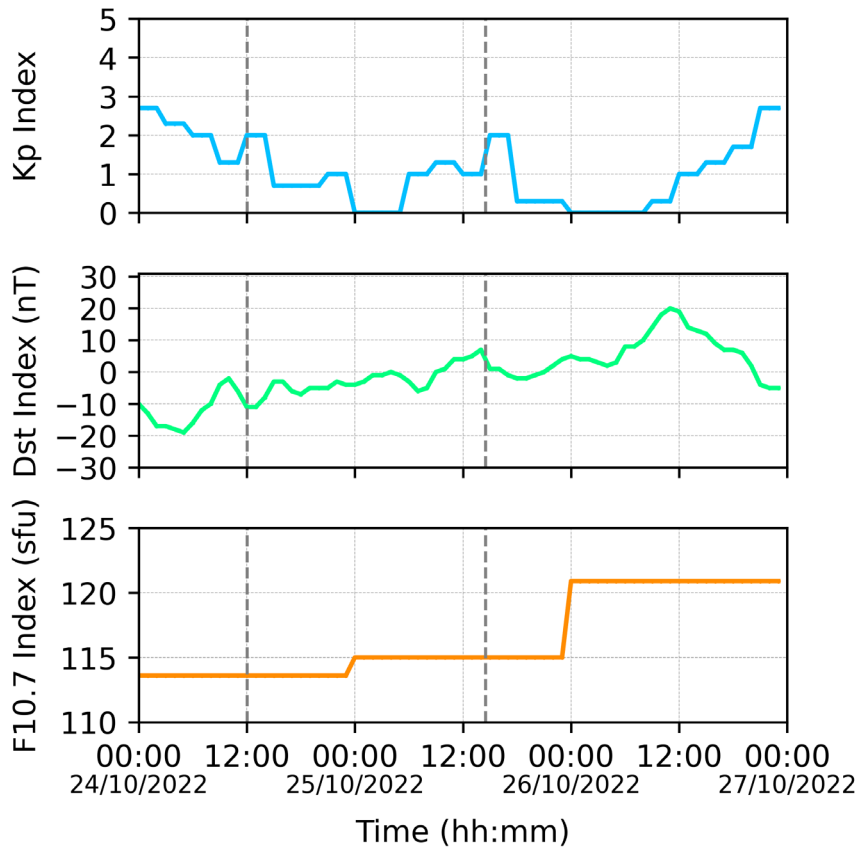


Figure 3. Daily ionospheric scintillation indicators: Kp index (top), Dst index (middle), and F10.7 index (bottom).

initial epoch was defined as the convergence time. In order to consider the results from different points of view, the convergence time, the number of reinitializing efforts for the solutions, and the ratio of the number of epochs with a value of 10 cm or less from the 2D positioning differences to the total number of epochs (after the convergence period) were calculated. All of these calculated values for the solutions are given in Table 7.

Using the values given in Figure 4, Table 6, and Table 7, conclusions were reached as described in the following subsections.

3.3.3.1. Points located in the Arctic region

For NABG (78.943°N, 11.857°E), the IGS CNES SSR solutions provided mean differences for 2D positioning of 4.4 cm, 3.9 cm, and 3.1 cm for GPS-only, Galileo-only, and GPS + Galileo constellations, respectively, with corresponding RMSE of ± 4.9 cm, ± 4.4 cm, and ± 3.8 cm. In terms of the height component, the mean differences were found to be 5.3 cm, 6.0 cm, and 7.2 cm for GPS-only, Galileo-only, and GPS + Galileo constellations, respectively, with corresponding RMSE of ± 9.8 cm, ± 8.8 cm, and ± 10.6 cm. The Galileo-only solutions from CNES had the

shortest convergence time of 10 min. In this solution, the reinitializing process occurred 3–4 times, and the ratio of epochs with position differences smaller than 10 cm to the whole solution was obtained as 94% for the GPS + Galileo constellations solution. This rate was higher than the rates obtained for the GPS-only and Galileo-only solutions.

The mean 2D positioning differences of RT-PPP based on NAVCAST products were 5.9 cm, 5.4 cm, and 5.5 cm for GPS-only, Galileo-only, and GPS + Galileo constellations, respectively, with corresponding RMSE of ± 6.4 cm, ± 6.2 cm, and ± 6.1 cm. Concerning the height component, the mean differences were found to be 4.4 cm, 2.7 cm, and 4.3 cm for GPS-only, Galileo-only, and GPS + Galileo constellations, respectively, with corresponding RMSE of ± 14.1 cm, ± 14.0 cm, and ± 8.6 cm. The shortest convergence time was 33 min for the Galileo-only solution. In this solution, reinitializing occurred 1–4 times, and the ratio of epochs with position differences smaller than 10 cm to the whole solution was obtained as 85% for the GPS + Galileo combined constellations.

For UTQI (71.323°N, 156.615°W), the mean differences for the CNES solution for 2D positioning were found

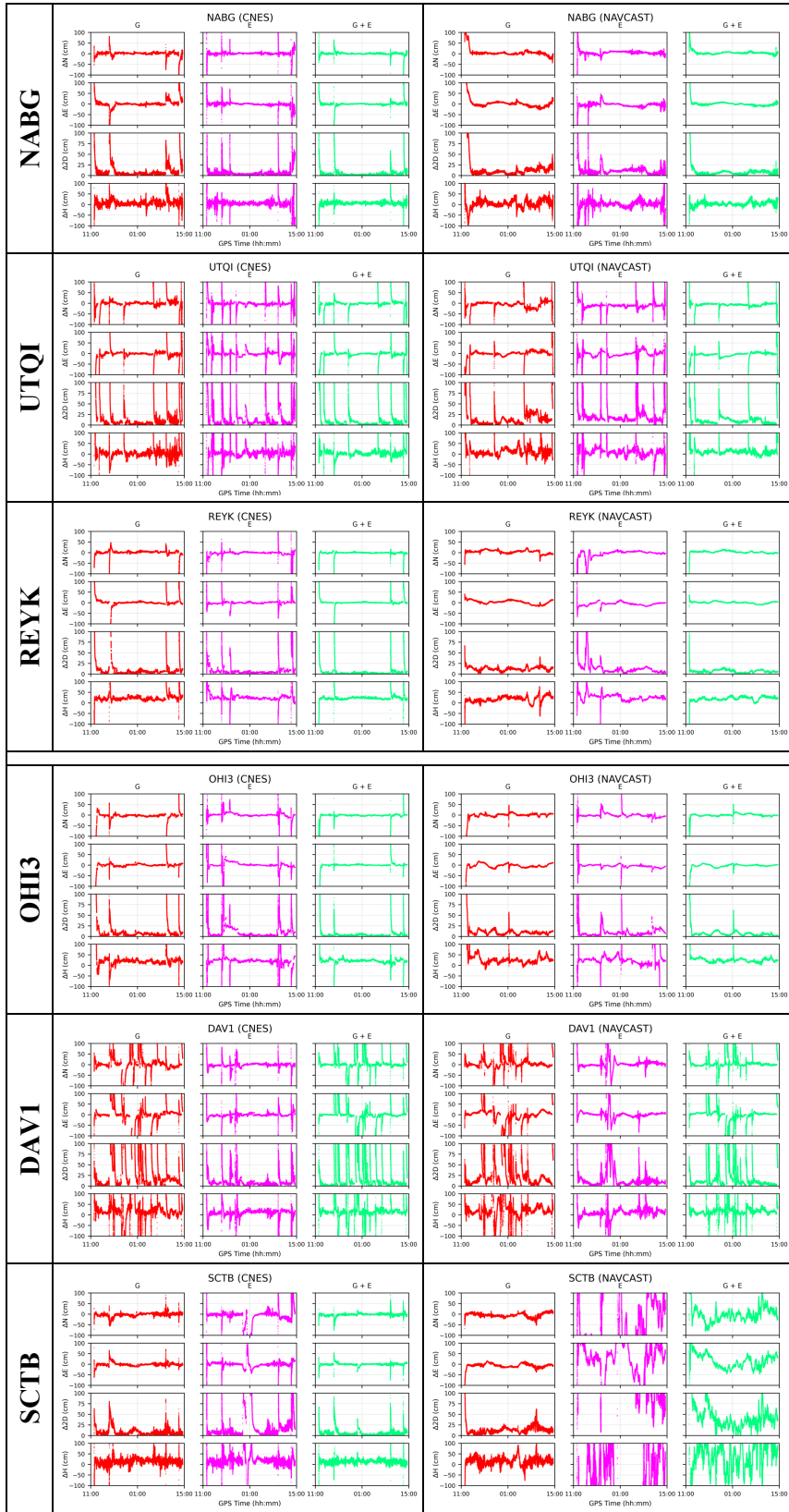


Figure 4. Coordinate differences between RT-PPP coordinates and corresponding known values.

Table 6. RT-PPP solution statistics.

Site	Constellation	RMSE (cm)		Site	Constellation	RMSE (cm)	
		2D	Height			2D	Height
NABG (78.943°N, 11.857°E)	CNES (G)	± 4.9	± 9.8	OH13 (63.321°S, 57.901°W)	CNES (G)	± 5.3	± 20.5
	CNES (E)	± 4.4	± 8.8		CNES (E)	± 3.8	± 21.7
	CNES (G+E)	± 3.8	± 10.6		CNES (G+E)	± 3.5	± 22.5
	NAVCAST (G)	± 6.4	± 14.1		NAVCAST (G)	± 6.8	± 30.2
	NAVCAST (E)	± 6.2	± 14.0		NAVCAST (E)	± 5.7	± 27.1
	NAVCAST (G+E)	± 6.1	± 8.6		NAVCAST (G+E)	± 5.3	± 25.3
UTQI (71.323°N, 156.615°W)	CNES (G)	± 5.5	± 9.4	DAV1 (68.577°S, 77.973°E)	CNES (G)	± 5.3	± 18.5
	CNES (E)	± 5.4	± 9.6		CNES (E)	± 5.5	± 15.7
	CNES (G+E)	± 5.4	± 8.0		CNES (G+E)	± 5.2	± 15.9
	NAVCAST (G)	± 5.3	± 15.1		NAVCAST (G)	± 6.3	± 22.5
	NAVCAST (E)	± 8.5	± 17.4		NAVCAST (E)	± 6.4	± 16.9
	NAVCAST (G+E)	± 6.6	± 11.4		NAVCAST (G+E)	± 6.2	± 18.2
REYK (64.139°N, 21.955°W)	CNES (G)	± 5.0	± 21.7	SCTB (77.849°S, 166.758°E)	CNES (G)	± 5.0	± 18.0
	CNES (E)	± 4.9	± 24.9		CNES (E)	± 5.5	± 18.6
	CNES (G+E)	± 3.2	± 22.7		CNES (G+E)	± 4.3	± 15.0
	NAVCAST (G)	± 7.3	± 24.6		NAVCAST (G)	± 7.0	± 23.8
	NAVCAST (E)	± 6.1	± 26.6		NAVCAST (E)	± 9.2	± 8.5
	NAVCAST (G+E)	± 6.1	± 22.2		NAVCAST (G+E)	± 6.4	± 53.5

to be 4.9 cm (± 5.5 cm RMSE), 4.9 cm (± 5.4 cm RMSE), and 4.6 cm (± 5.4 cm RMSE) for the GPS-only, Galileo-only, and GPS + Galileo constellations, respectively. For the height component, the mean differences were 2.2 cm (± 9.4 cm RMSE), 4.8 cm (± 9.6 cm RMSE), and 4.2 cm (± 8.0 cm RMSE) for the GPS-only, Galileo-only, and GPS + Galileo constellations, respectively. In this alternative, the shortest convergence time was obtained as 32 min for the Galileo-only solution. In this solution, reinitializing occurred 7–9 times, and the ratio of epochs with position differences smaller than 10 cm to the whole solution was obtained as 76% for the GPS + Galileo combined constellations.

For the NAVCAST-based solutions, the mean differences of 2D positioning were 4.6 cm (± 5.3 cm RMSE), 8.3 cm (± 8.5 cm RMSE), and 6.1 cm (± 6.6 cm RMSE) for GPS-only, Galileo-only, and GPS + Galileo constellations, respectively. The mean height differences of the RT-PPP solutions were 7.1 cm (± 15.1 cm RMSE), 7.3 cm (± 17.4 cm RMSE), and 9.5 cm (± 11.4 cm RMSE) for GPS-only, Galileo-only, and GPS + Galileo constellations, respectively. The minimum convergence time for NAVCAST solutions was obtained as 32 min for the GPS + Galileo constellations. In this solution, reinitializing occurred 4–8 times, and the ratio of epochs with position differences

smaller than 10 cm to the whole solution was obtained as 61% for the GPS + Galileo combined constellations.

For REYK (64.139°N, 21.955°W), the mean 2D positioning differences of the RT-PPP solution from IGS CNES SSR products were 4.3 cm, 4.4 cm, and 2.5 cm for GPS-only, Galileo-only, and GPS + Galileo constellations, respectively, with corresponding RMSE of ± 5.0 cm, ± 4.9 cm, and ± 3.2 cm. The mean height differences after the convergence period were 20.6 cm (± 21.7 cm RMSE), 23.7 cm (± 24.9 cm RMSE), and 22.1 cm (± 22.7 cm RMSE) for GPS-only, Galileo-only, and GPS + Galileo constellations, respectively. The minimum convergence time for the real-time PPP solution was 27 min for the GPS + Galileo combination. In this solution, reinitializing occurred 3–4 times, and the ratio of epochs with position differences smaller than 10 cm to the whole solution was obtained as 96% for the GPS + Galileo combined constellations.

The mean differences for 2D positioning based on NAVCAST products were 7.1 cm, 5.7 cm, and 5.5 cm for GPS-only, Galileo-only, and GPS + Galileo constellations, respectively. The corresponding RMSE values of the RT-PPP solutions were ± 7.3 cm, ± 6.1 cm, and ± 6.1 cm. For the height component, the mean differences were 20.3 cm (± 24.6 cm RMSE), 24.4 cm (± 26.6 cm RMSE), and 20.6 cm (± 22.2 cm RMSE) for GPS-only, Galileo-only, and GPS

Table 7. Convergence time, number of reinitializations, and accepted solution ratio for all solutions.

Site	Constellation	CNES			NAVCAST		
		Ratio (%) *	Conv. time (min.)	Number of reinit. **	Ratio (%) *	Conv. time (min.)	Number of reinit. **
NABG	G	81	33	3	59	103	1
	E	90	10	4	51	33	4
	G+E	94	21	3	85	52	1
UTQI	G	61	44	7	49	115	6
	E	63	32	9	8	44	8
	G+E	76	36	7	61	32	4
REYK	G	84	42	3	28	37	1
	E	87	60	4	50	63	3
	G+E	96	27	3	87	7	0
OHI3	G	85	74	3	59	58	1
	E	68	40	3	75	55	3
	G+E	95	31	3	87	40	1
DAV1	G	39	38	11	32	19	14
	E	80	38	5	62	86	7
	G+E	67	23	15	61	18	12
SCTB	G	80	36	4	39	35	1
	E	52	7	5	0	427	-
	G+E	88	10	4	5	468	10

* Ratio of the number of epochs with a value of 10 cm or less from the 2D positioning differences to the total number of epochs.

** Numbers of reinitializations were visually derived from figures.

+ Galileo constellations, respectively. The minimum convergence time of the RT-PPP solution using SSR products from NAVCAST was 7 min for the GPS + Galileo combination. In this solution, reinitializing occurred 0–3 times, and the ratio of epochs with position differences smaller than 10 cm to the whole solution was obtained as 87% for the GPS + Galileo combined constellations.

3.3.3.2. For points located in the Antarctic region

For OHI3 (63.321°S, 57.901°W), the mean 2D differences from CNES solutions were 4.8 cm (± 5.3 cm RMSE), 3.2 cm (± 3.8 cm RMSE), and 2.9 cm (± 3.5 cm RMSE) for GPS-only, Galileo-only, and GPS + Galileo constellations, respectively. The mean height differences were 19.3 cm (± 20.5 cm RMSE), 20.9 cm (± 21.7 cm RMSE), and 21.6 cm (± 22.5 cm RMSE). The shortest convergence time for the solutions based on CNES products was 31 min (GPS + Galileo solution). In this solution, reinitializing occurred 3 times, and the ratio of epochs with position differences smaller than 10 cm to the whole solution was obtained as 95% for the GPS + Galileo combined constellations.

Based on the NAVCAST solutions, the mean 2D posi-

tioning differences were 6.4 cm for GPS-only, 5.3 cm for Galileo-only, and 4.8 cm for GPS + Galileo constellations with corresponding RMSE of ± 6.8 cm, ± 5.7 cm, and ± 5.3 cm. The height solutions produced mean differences of 26.6 cm for GPS-only, 22.5 cm for Galileo-only, and 24.0 cm for the GPS + Galileo combination with corresponding RMSE of ± 30.2 cm, ± 27.1 cm, and ± 25.3 cm. The shortest convergence time of the RT-PPP solution using SSR products from NAVCAST was 40 min (GPS + Galileo solution). In this solution, reinitializing occurred 1–3 times, and the ratio of epochs with position differences smaller than 10 cm to the whole solution was obtained as 87% for the GPS + Galileo combined constellations.

For DAV1 (68.577°S, 77.973°E), the CNES provided 2D mean differences of 4.6 cm, 5.0 cm, and 4.4 cm for GPS-only, Galileo-only, and GPS + Galileo constellations with RMSE of ± 5.3 cm, ± 5.5 cm, and ± 5.2 cm, respectively. The mean differences for the height component were found to be 15.5 cm (± 18.5 cm RMSE) for GPS-only, 13.5 cm (± 15.7 cm RMSE) for Galileo-only, and 14.2 cm (± 15.9 cm RMSE) for GPS + Galileo constellations. For this product, the shortest convergence time was found as 23

min for the GPS + Galileo solution. In this solution, reinitializing occurred 5–15 times, and the ratio of epochs with position differences smaller than 10 cm to the whole solution was obtained as 67% for the GPS + Galileo combined constellations.

The mean 2D differences based on the NAVCAST SSR products were 5.7 cm (± 6.3 cm RMSE) for GPS-only, 5.9 cm (± 6.4 cm RMSE) for Galileo-only, and 5.7 cm (± 6.2 cm RMSE) for GPS + Galileo constellations. Concerning the height component, the mean differences were found to be 18.8 cm, 13.4 cm, and 15.8 cm for GPS-only, Galileo-only, and GPS + Galileo constellations, respectively, with corresponding RMSE of ± 22.5 cm, ± 16.9 cm, and ± 18.2 cm. The shortest convergence time was 18 min for the GPS + Galileo constellations among all the solutions. In this solution, reinitializing occurred 7–14 times, and the ratio of epochs with position differences smaller than 10 cm to the whole solution was obtained as 61% for the GPS + Galileo combined constellations.

For SCTB (77.849°S, 166.758°E), the mean differences for 2D positioning were 4.3 cm (± 5.0 cm RMSE) for GPS-only, 4.8 cm (± 5.5 cm RMSE) for Galileo-only, and 3.6 cm (± 4.3 cm RMSE) for GPS + Galileo constellations. The mean height differences of the RT-PPP solutions were 12.7 cm (± 18.0 cm RMSE), 15.4 cm (± 18.6 cm RMSE), and 13.0 cm (± 15.0 cm RMSE) for GPS-only, Galileo-only, and GPS + Galileo constellations, respectively. The Galileo-only solution from CNES had the shortest convergence time of about 7 min. In this solution, reinitializing occurred 4–5 times, and the ratio of epochs with position differences smaller than 10 cm to the whole solution was obtained as 88% for the GPS + Galileo combined constellations.

The NAVCAST-based solutions produced 2D mean differences of 6.6 cm (± 7.0 cm RMSE) for GPS-only, 9.2

cm (± 9.2 cm RMSE) for Galileo-only, and 5.8 cm (± 6.4 cm RMSE) for GPS + Galileo constellations. For the height component, the mean differences were 15.5 cm, 6.2 cm, and 34.4 cm for the GPS-only, Galileo-only, and GPS + Galileo constellations, with RMSE of ± 23.8 cm, ± 8.5 cm, and ± 53.5 cm, respectively. The shortest convergence time was found to be 35 min for the GPS-only solution. In this solution, reinitializing occurred 1–10 times, and the ratio of epochs with position differences smaller than 10 cm to the whole solution was obtained as 5% for the GPS + Galileo combined constellations.

Considering that the solutions obtained with CNES products used the PPP-AR solution strategy, it was found that the GPS ambiguities were resolved with ratios of 92.4%, 84.7%, 92.4%, 92%, 62%, and 92.4% for the NABG, UTQI, REYK, OHI3, DAV1, and SCTB stations, respectively. The same ratios were also found for GPS + Galileo combined solutions. The ambiguity resolution percentage was almost the same for all Galileo solutions except for the DAV1 and SCTB stations. However, the ambiguities of Galileo observations were resolved as a float at the SCTB station. One of the important factors affecting the solution is the availability of observations and SSR products. The lack of observations and SSR products may affect the positioning performance adversely. As a result of the analysis of these two issues in our test data, approximately 0.5%, 3.5%, 0.5%, 4%, 2%, and 0.5% of the observations for the NABG, UTQI, REYK, OHI3, DAV1, and SCTB stations, respectively, were missing in the 26.5-h observation session. This might have been caused by a problem with the data transfer.

After excluding these missing epochs, the availability of correction data for GPS and Galileo satellites through the measurement period were plotted, as shown in Figure 5. All of these calculations were carried out with Python programming language-based in-house software.

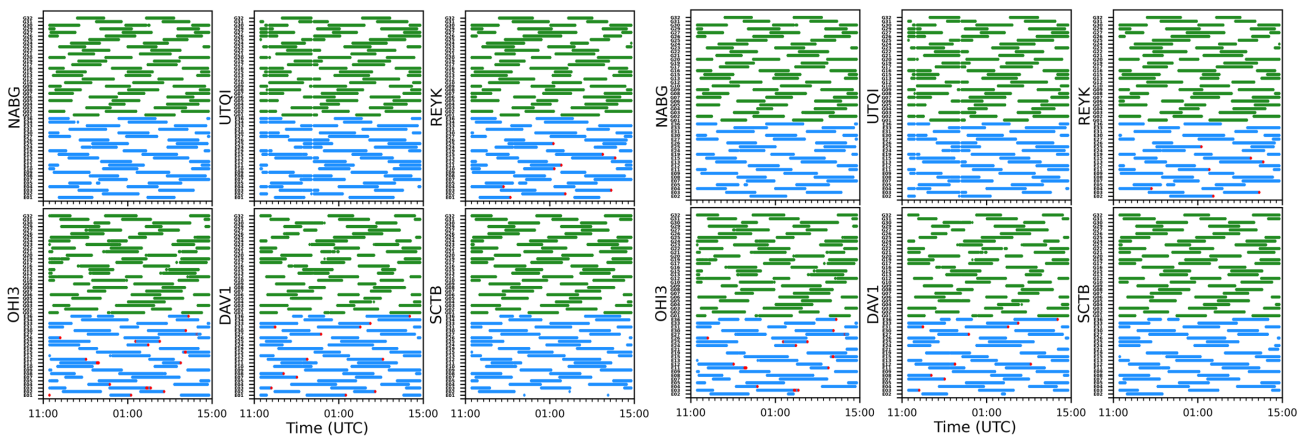


Figure 5. Real-time correction data availability during the test measurements. Left: For CNES solutions; right: for NAVCAST solutions (green: available GPS satellite corrections; blue: available Galileo satellite corrections; red: epochs without corrections).

As seen in Figure 5, the availability of correction data for GPS satellites was 100%. In addition, the availability of SSR corrections for Galileo satellites was found to be over 99.5%.

4. Results and discussion

According to the analysis of the GNSS dataset processing results given in the previous section, the following general remarks can be made:

- The GPS and Galileo combination increased the total number of satellites. While additional satellite systems increased the number of satellites, observation geometry, and satellite availability, the positioning accuracy also generally increased. The combination of GPS and Galileo constellations improved the integrity and coverage. This is especially important in the GNSS-challenging environment of the polar regions.
- In terms of PDOP values that reflect the geometric quality of the observed GNSS satellite configuration, the combination of GPS and Galileo observations produced PDOP between 1.3 and 1.5 as mean values. The PDOP values in the Arctic region were generally very similar to those in the Antarctic region. According to Table 5, the combined constellations made a significant contribution compared to the single satellite system.
- There were no satellites observed in the zenith direction, leaving a hole in the sky over the stations due to the orbital planes of the used GNSS satellites. This caused better horizontal but worse vertical satellite geometry compared to mid- and low-latitude region applications (Jensen and Sicard, 2010). This particularly influenced the height component, and depending on this, the accuracy of the height component was found to be worse than that at middle and lower latitudes. (Jensen and Sicard, 2010)
- From all solutions' results of processing the GNSS datasets of the polar regions, it was concluded that the RT-PPP-derived coordinates from CNES solutions agreed with the known coordinates between 2.5 and 5.0 cm and between 2.2 and 23.7 cm as mean values for 2D position and height, respectively, after the initialization period. The RMSE value obtained from calculated and reference coordinates reached ± 5.5 cm and ± 24.9 cm as maximum values for the 2D position and height components, respectively. The convergence times were found to be between 7 min and 74 min. In general, when the mean 2D differences were examined, it was seen that the GPS + Galileo solution improved the GPS-only and Galileo-only solutions while also producing the best solution. For the height component, the GPS + Galileo combination did not provide an improvement, and GPS-only produced the best solution (with one exception).
- For NAVCAST solutions, the differences were found to be between 4.6 and 9.2 cm and between 2.7 and 34.4 cm for 2D position and height, respectively, for all solutions after excluding the initialization period. The RMSE values reached ± 9.2 cm and ± 53.5 cm as maximum values for the 2D position and height components, respectively. The convergence times were found to be between 7 min and 115 min (with two abnormal exceptions for the SCTB station). The mean 2D differences were examined in general, and it could be said that the GPS + Galileo solution produced the best solutions compared to single-system solutions. For the height component, similar to CNES solutions, the GPS + Galileo combination did not provide an improvement, and Galileo-only produced the best solution in most cases.
- Based on all RT-PPP solutions using CNES SSR precise products, the results showed that the combination of GPS and Galileo constellations provided better 2D positioning accuracy with levels of a few centimeters compared to stand-alone constellations in terms of RMSE. On the contrary, for the height component, the GPS + Galileo combination did not improve the accuracy for most of the solutions. For NAVCAST products, except for the solutions from the UTQI station, the GPS + Galileo combination increased the 2D positioning accuracy compared to the GPS-only solutions. For the height component, the same situation was observed, except for the SCTB solutions. Considering the RMSE values of the solutions, it was seen that the CNES solutions produced horizontal position accuracy of 3–5 cm and height accuracy of 1–2 dm. On the other hand, NAVCAST solutions produced 2D position accuracy of 5–9 cm and height accuracy of 1–5 dm. From this point of view, it was seen that CNES solutions provided higher accuracy than NAVCAST solutions. It should be remembered that the solutions obtained with CNES products were PPP-AR, while the solutions obtained with NAVCAST products were PPP-float solutions. Therefore, it was concluded that the CNES RT-PPP-AR solution achieved better accuracy than NAVCAST.
- It was observed that lower accuracies were generally obtained for the height component. This is thought to be due to the negative effect of the satellite configuration on height determination accuracy, as explained above.
- Considering the convergence times of the solutions, although quite different values were obtained, GPS-only solutions had a longer convergence time than Galileo-only and GPS + Galileo combination solutions, except for a few of them.
- Although the GPS and Galileo combination achieved

quite stable solutions compared to a single constellation, in general, there were fluctuations in the differences obtained from both solutions (Figure 4). One of the most important reasons for the occurrence of these unstable parts was that the solutions required reconvergence processes. This situation was caused mainly by the interruption of raw observations and was seen when the limited number of visible satellites and corresponding PDOP values were high. It should be remembered that the performance of RT-PPP solutions is strongly affected by the availability of correction data and raw observations.

5. Conclusion

In this study, RT-PPP performance was evaluated in terms of accuracy and convergence time in the harsh environmental and extreme atmospheric conditions of polar regions using different real-time service products and different satellite configurations. According to the results, compared to conventional RTK techniques, RT-PPP was more advantageous and more suitable for accurate real-time positioning. The findings of this study have shown that the RT-PPP technique provides 3D positioning accuracy varying in the order of centimeters to decimeters using only one GNSS receiver in polar regions. The obtained results proved that the accuracy highly depended on the SSR correction and the satellite configuration used in the solution. This attainable accuracy can meet the requirements of many Arctic and Antarctic projects, including studies on mapping, glacial monitoring, geodynamics, climate and atmosphere, plate kinematics, marine biology, seismology, the environment, and so on. Real-time positioning is very important, especially in applications such as monitoring deformations in the region, monitoring glaciers, and creating early warning systems, autonomous navigation, and UAV surveys, and this method stands out as a very effective alternative.

Today, the RT-PPP technique has almost entirely replaced the classical differential GNSS positioning technique due to its accuracy, ease of use, economic benefits, and many other advantages. However, the method also has some limitations and deficiencies. In this context, it is im-

portant to emphasize that a robust internet connection or cellular coverage to receive correction products has been an important key factor for stable, continuous, and seamless real-time positioning. At the same time, the telecommunication capabilities in the polar regions, and especially in Antarctica, are quite limited and poor. This important problem can be solved by using satellite-based internet service providers with global coverage, such as SpaceX's Starlink service. On the other hand, communication problems can also be eliminated if the SSR products used in RT-PPP are provided by communication satellites over the L-band rather than the internet. However, it should be emphasized here that the coverage of most geostationary satellites does not include the upper part of the polar regions due to the architecture of their orbits (generally available between 75°N and 78°S). This situation causes communication satellites to be seen at very low elevation angles or even not to be seen at all.

On the other hand, the convergence time issue, which is one of the most important limitations of the classical PPP technique, is still an important problem in real-time PPP. When the values given in Table 7 are examined, it is seen that the convergence time values of the solutions vary in a range from a few minutes to several hours depending on the used real-time corrections and GNSS satellite constellations. More importantly, the RT-PPP solution requires reinitialization as a result of data/correction interruptions due to various reasons; thus, the positioning discontinuity problem was the most important problem we encountered in this study.

Acknowledgments

The preliminary results of this study were presented at the 6th National Polar Sciences Workshop held in Trabzon, Türkiye, on 30 November 2022. The authors gratefully acknowledge the IGS and NAVCAST RTS for providing real-time SSR streams and GNSS data. CNES is also appreciated for providing the PPP-WIZARD software. We also sincerely thank the editor and the anonymous reviewers for their comprehensive review and constructive comments and suggestions that significantly contributed to improving the manuscript.

References

- Alkan RM (2021). Cm-level high accurate point positioning with satellite-based GNSS correction service in dynamic applications. *Journal of Spatial Science* 66 (2): 351-359. <https://doi.org/10.1080/14498596.2019.1643795>
- Alkan RM, Erol S, Mutlu B (2022). Real-time multi-GNSS precise point positioning using IGS-RTS products in Antarctic region. *Polar Science* 32: 100844. <https://doi.org/10.1016/j.polar.2022.100844>
- An X, Ziebold R, Lass C (2023). From RTK to PPP-RTK: Towards real-time kinematic precise point positioning to support autonomous driving of inland waterway vessels. *GPS Solutions* 27: 86. <https://doi.org/10.1007/s10291-023-01428-2>
- Anantakarn K, Witchayangkoon B (2019). Accuracy assessment of L-Band Atlas GNSS System in Thailand. *International Transaction Journal of Engineering, Management, & Applied Sciences & Technology* 10 (1): 91-98. <https://doi.org/10.14456/ITJEMAST.2019.9>

- Atiz OF, Alcay S, Ogutcu S, Bugdayci I (2023). Comparative analysis of real-time precise point positioning method in terms of positioning and zenith tropospheric delay estimation. *Survey Review* 55 (388): 55-67. <https://doi.org/10.1080/00396265.2021.2001627>
- Banville S (2020). CSRS-PPP Version 3: Tutorial. Edmonton, AB, Canada: Canadian Geodetic Survey, Surveyor General Branch, Natural Resources Canada. Available at: https://webapp.csrscs.nrcan-rncan.gc.ca/geod/tools-outils/sample_doc_files/V3/NRCAN%20CSRS-PPP-v3_Tutorial%20EN.pdf [last accessed September 2, 2023].
- Bezioglu M, Karadeniz B, Yigit CO, Dindar AA, Tiryakioğlu I et al. (2021). Real-time precise point positioning (RT-PPP) for capturing seismic waveform and coseismic displacement. In: 6th International Conference on Earthquake Engineering and Seismology; Gebze, Türkiye. pp. 861-871.
- Bezioglu M, Yigit CO, El-Mowafy A (2019). Kinematic PPP-AR in Antarctic: comparing methods for precise positioning. *Sea Technology* 60: 20-23.
- Cheng Q, Zhang Y, Chen J (2022). Evaluation of BDS-2/BDS-3 precise point positioning performance in polar region. *Lecture Notes in Electrical Engineering* 910: 161-172. https://doi.org/10.1007/978-981-19-2576-4_14
- De Jong K, Goode M, Liu X, Stone M (2014). Precise GNSS positioning in Arctic regions. In: OTC Arctic Technology Conference; Houston, Texas, USA. <https://doi.org/10.4043/24651-MS>
- Di M, Guo B, Ren J, Wu X, Zhang Z et al. (2022). GNSS real-time precise point positioning in Arctic Northeast Passage. *Journal of Marine Science and Engineering* 10 (10): 1345. <https://doi.org/10.3390/jmse10101345>
- Ding W, Teferle FN, Kazmierski K, Laurichesse D, Yuan Y (2017). An evaluation of real-time troposphere estimation based on GNSS precise point positioning. *Journal of Geophysical Research: Atmospheres* 122: 2779-2790. <https://doi.org/10.1002/2016JD025727>
- Elmezayen A, El-Rabbany A (2019). Real-time GPS/Galileo precise point positioning using NAVCAST real-time corrections. *Positioning* 10 (3): 35-49. <https://doi.org/10.4236/pos.2019.103003>
- Elmezayen A, El-Rabbany A (2020). Assessment of NAVCAST precise orbit and clock products for real-time GPS/Galileo PPP. In: FIG Working Week 2020, Smart Surveyors for Land and Water Management; Amsterdam, the Netherlands.
- Erol S, Alkan RM, Mutlu B (2023). The assessment of multi-GNSS RT-PPP services in Antarctic region. *Arctic Journal* 76 (3) (in press).
- Fan S, Fan Y, Wu X, Zheng K, Xu D et al. (2021). Analysis of the BDS-3 complete system on positioning performance in polar region. *Lecture Notes in Electrical Engineering* 773: 174-186. https://doi.org/10.1007/978-981-16-3142-9_16
- Gazzino C, Blot A, Bernadotte E, Jayle T, Laymand M et al. (2023). The CNES solutions for improving the positioning accuracy with post-processed phase biases, a snapshot mode, and high-frequency Doppler measurements embedded in recent advances of the PPP-WIZARD Demonstrator. *Remote Sensing* 15 (17): 4231. <https://doi.org/10.3390/rs15174231>
- Grinter T, Roberts C, Janssen V (2020). Ambiguity-resolved real-time precise point positioning as a potential fill-in service for sparse CORS networks. *Journal of Surveying Engineering* 146 (2): 04020007. [https://doi.org/10.1061/\(ASCE\)SU.1943-5428.0000314](https://doi.org/10.1061/(ASCE)SU.1943-5428.0000314)
- Jensen ABO, Sicard JP (2010). Challenges for positioning and navigation in the Arctic. *Coordinates* 6 (10): 10-13.
- Jin X, Ma R, Wang J, Chu R, Zheng S et al. (2023). Analysis on positioning performance of BDS-3 system in polar region. In: *Advances in Guidance, Navigation and Control: Proceedings of 2022 International Conference on Guidance, Navigation and Control*; Singapore. pp. 572-583. https://doi.org/10.1007/978-981-19-6613-2_57
- Junior PSDO (2017). Definition and implementation of a new service for precise GNSS positioning. PhD, São Paulo State University, São Paulo, Brazil.
- Laurichesse D, Privat A (2015). An open-source PPP client implementation for the CNES PPP-WIZARD Demonstrator. In: *Proceedings of the 28th International Technical Meeting of the Satellite Division of The Institute of Navigation*; Tampa, FL, USA. pp. 2780-2789.
- Li M, Xu T, Flechtner F, Förste C, Lu B et al. (2019a). Improving the performance of multi-GNSS (Global Navigation Satellite System) ambiguity fixing for airborne kinematic positioning over Antarctica. *Remote Sensing* 11 (8): 992. <https://doi.org/10.3390/rs11080992>
- Li M, Xu T, Lu B, He K (2019b). Multi-GNSS precise orbit positioning for airborne gravimetry over Antarctica. *GPS Solutions* 23 (2): 53. <https://doi.org/10.1007/s10291-019-0848-9>
- Li W, Song S, Zhou W, Cheng N, Yu C (2022). Investigating the impacts of ionospheric irregularities on precise point positioning over China and its mechanism. *Space Weather* 20 (11): e2022SW003236. <https://doi.org/10.1029/2022SW003236>
- Li X, Huang J, Li X, Shen Z, Han J et al. (2022a). Review of PPP-RTK: Achievements, challenges, and opportunities. *Satellite Navigation* 3: 28. <https://doi.org/10.1186/s43020-022-00089-9>
- Li X, Wang B, Li X, Huang J, Lyu H et al. (2022b). Principle and performance of multi-frequency and multi-GNSS PPP-RTK. *Satellite Navigation* 3: 7. <https://doi.org/10.1186/s43020-022-00068-0>
- Lipatnikov LA, Shevchuk SO (2019). Cost Effective Precise Positioning with GNSS. Copenhagen, Denmark: International Federation of Surveyors.
- Liu T, Jiang W, Laurichesse D, Chen H, Liu X et al. (2020). Assessing GPS/Galileo real-time precise point positioning with ambiguity resolution based on phase biases from CNES. *Advances in Space Research* 66 (4): 810-825. <https://doi.org/10.1016/j.asr.2020.04.054>
- Poole I (2002). Understanding solar indices. *QST* 86 (9): 38-40.
- Qu L, Du Y, Wang H, Jiang W, Wang L (2023). Multi-constellation and multi-frequency precise point positioning with fast ambiguity resolution on a global scale. *Measurement* 211: 112642. <https://doi.org/10.1016/j.measurement.2023.112642>

- Savchyn I, Brusak I, Tretyak K (2023). Analysis of recent Antarctic plate kinematics based on GNSS data. *Geodesy and Geodynamics* 14 (2): 99-110. <https://doi.org/10.1016/j.geog.2022.08.004>
- Teunissen PJG (2021). GNSS precise point positioning. In: Morton YTJ, van Diggelen F, Spilker JJ Jr, Parkinson BW, Lo S et al. (editors). *Position, Navigation, and Timing Technologies in the 21st Century: Integrated Satellite Navigation, Sensor Systems, and Civil Applications*. New York, NY, USA: IEEE, pp. 503-528. <https://doi.org/10.1002/9781119458449.ch20>
- Url-1. IGS RTS Contributors + Providers, <https://igs.org/rts/contributors> [last accessed September 2, 2023].
- Url-3. Precise Point Positioning, <https://webapp.csrscs.nrcan-ncan.gc.ca/geod/tools-outils/ppp.php> [last accessed September 2, 2023].
- Wang Z, Li Z, Wang L, Wang X, Yuan H (2018). Assessment of multiple GNSS real-time SSR products from different analysis centers. *ISPRS International Journal of Geo-Information* 7 (3): 85. <https://doi.org/10.3390/ijgi7030085>
- Xu Y, Yang Y, Xu G (2012). Precise determination of GNSS trajectory in the Antarctic airborne kinematic positioning. *Lecture Notes in Electrical Engineering* 159: 95-105. https://doi.org/10.1007/978-3-642-29187-6_9
- Yu D, Ji B, Liu Y, Wu S, Li H et al. (2023). Performance assessment of RTPPP positioning with SSR corrections and PPP-AR positioning with FCB for multi-GNSS from MADOCA products. *Advances in Space Research* 71 (6): 2924-2937. <https://doi.org/10.1016/j.asr.2022.11.039>
- Zhao J, An J, Wang Z, Ai S, Zhu L et al. (2022). Signal quality and positioning performance of GPS/BDS-3/GLONASS/Galileo in polar regions. *Advances in Space Research* 69 (6): 2541-2554. <https://doi.org/10.1016/j.asr.2021.12.032>